An Observational Estimate of Inferred Ocean Energy Divergence

KEVIN E. TRENBERTH AND JOHN T. FASULLO

National Center for Atmospheric Research, Boulder, Colorado*

(Manuscript received 2 May 2007, in final form 25 September 2007)

ABSTRACT

Monthly net surface energy fluxes (F_S) over the oceans are computed as residuals of the atmospheric energy budget using top-of-atmosphere (TOA) net radiation (R_T) and the complete atmospheric energy (A_E) budget tendency ($\delta A_E/\delta t$) and divergence ($\nabla \cdot \mathbf{F}_A$). The focus is on TOA radiation from the Earth Radiation Budget Experiment (ERBE) (February 1985–April 1989) and the Clouds and Earth's Radiant Energy System (CERES) (March 2000–May 2004) satellite observations combined with results from two atmospheric reanalyses and three ocean datasets that enable a comprehensive estimate of uncertainties. Surface energy flux departures from the annual mean and the implied annual cycle in "equivalent ocean energy content" are compared with the directly observed ocean energy content (O_E) and tendency ($\delta O_E/\delta t$) to reveal the inferred annual cycle of divergence ($\nabla \cdot \mathbf{F}_O$). In the extratropics, the surface flux dominates the ocean energy tendency, although it is supplemented by ocean Ekman transports that enhance the annual cycle in ocean heat content. In contrast, in the tropics, ocean dynamics dominate O_E variations throughout the year in association with the annual cycle in surface wind stress and the North Equatorial Current. An analysis of the regional characteristics of the first joint empirical orthogonal function (EOF) of F_S, $\delta O_E/\delta t$, and $\nabla \cdot \mathbf{F}_O$ is presented, and the largest sources of uncertainty are attributed to variations in O_E. The mean and annual cycle of zonal mean global ocean meridional heat transports are estimated. The annual cycle reveals the strongest poleward heat transports in each hemisphere in the cold season, from November to April in the north and from May to October in the south, with a substantial across-equatorial transport, exceeding 4 PW in some months. Annual mean results do not differ greatly from some earlier estimates, but the sources of uncertainty are exposed. Comparison of annual means with direct ocean observations gives reasonable agreement, except in the North Atlantic, where transports from the ocean transects are slightly greater than the estimates presented here.

1. Introduction

The oceans play a major role in moderating climate. In midlatitudes, energy absorbed by the oceans in summer is released to the atmosphere in winter, thus reducing the annual cycle in surface temperatures relative to those over land. Moreover, the advection of energy from the oceans also moderates the seasonal cycle over land where maritime influences prevail. Relative to the oceans, the atmosphere's capacity to store energy is small and equivalent to that of about 3.5 m of the ocean if their associated proportion of global coverage is considered. Because the main movement of energy in the land and ice components is by conduction, only very limited masses are involved in changes on annual time scales. Moreover, water has a much higher specific heat than dry land by about a factor of 4.5 or so. Accordingly, it is the oceans, through their total mass, heat capacity, and movement of energy by turbulence, convection, and advection, that have an enormous impact on the global energy budget, which can vary significantly on annual and longer time scales (Trenberth and Stepaniak 2004).

The net radiative flux (R_T) at the top of the atmosphere (TOA) on longer-than-annual time scales is mostly balanced by transports of energy by the atmosphere and ocean, and local upward surface energy fluxes (F_S) are largely offset by the ocean's divergent energy transport ($\nabla \cdot \mathbf{F}_O$) (Trenberth and Caron 2001). In contrast, for the annual cycle in midlatitudes the

* The National Center for Atmospheric Research is sponsored by the National Science Foundation.

Corresponding author address: Kevin E. Trenberth, National Center for Atmospheric Research, P.O. Box 3000, Boulder, CO 80307-3000.
E-mail: trenbert@ucar.edu

DOI: 10.1175/2007JPO3833.1

© 2008 American Meteorological Society

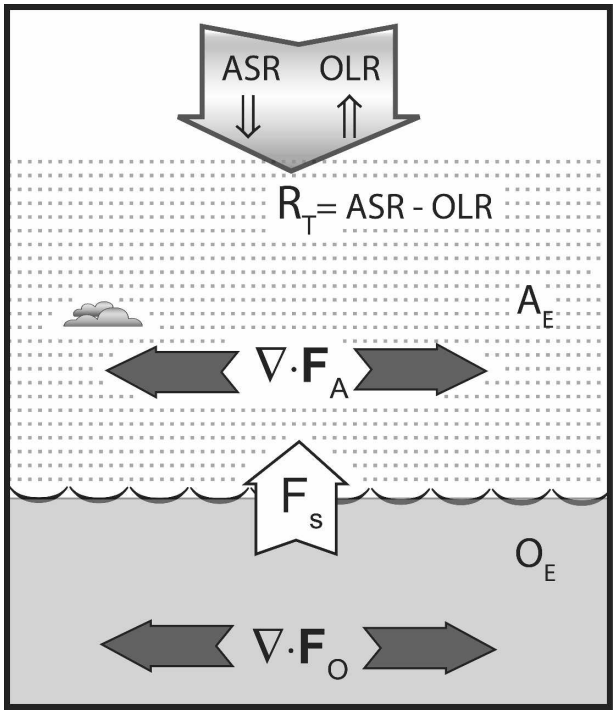

FIG. 1. Schematic is shown of the main energy quantities addressed in this paper. The incoming radiation at the TOA R_T (directed down) consists of the absorbed solar radiation (ASR) minus the outgoing longwave radiation (OLR). The vertically integrated atmospheric energy A_E and the ocean energy O_E change in response to the heating or the net surface energy flux (directed upward) F_S, or the energy is transported by winds in the atmosphere and currents in the ocean to provide divergence of atmospheric ($\nabla \cdot \mathbf{F}_A$) and oceanic ($\nabla \cdot \mathbf{F}_O$) energy.

dominant ocean response is the uptake and release of energy, with changes in ocean energy divergence being secondary (Jayne and Marotzke 2001). Here we begin by providing an estimate of the annual cycle in equivalent ocean energy content based on F_S alone. The term "equivalent" is used because it neglects the influence of heat transports. While the sparseness of ocean observations is a major constraint on our understanding of its energy budget, to the extent that reliable estimates of both actual and equivalent ocean energy content can be made, their differences can be interpreted as the result of the divergence of heat transports. Accordingly, we compute this residual for the mean annual cycle and annual mean. Figure 1 provides a schematic of the main energy components included in this study.

The main source of information on ocean energy content (O_E) comes from ocean temperature profiles compiled into datasets and analyzed in atlases. Previous analyses of O_E include both regional (e.g., Moisan and Niiler 1998) and global estimates using the *World Ocean Atlas* (*WOA*) *1994* (Levitus 1984, 1987; Levitus and Antonov 1997) and *WOA 2001* (Antonov et al. 2004). Recently, an update of these fields has been made available in the *WOA 2005* (Locarnini et al. 2006). These estimates start from the monthly analyses of the basic observations gridded into 1° squares at standard depth levels and are integrated in depth from the surface to 275 m. Despite the increasing volume of data incorporated into successive versions of the *WOA*, over some parts of the ocean either very few or no observations have been made at some times of the year (notably over the wintertime southern oceans), and consequently sampling errors are large so that the spatial patterns of O_E (Levitus and Antonov 1997) contain spurious noise. The recent availability of data from the Argo floats will improve the sampling of the southern oceans greatly; however, it will be several years before an extended data record is made available, and the reliability of data processing remains an ongoing issue (Willis et al. 2007).

Interannual temperature anomalies in the ocean can penetrate below 275 m (Levitus and Antonov 1997) into the thermocline through subduction processes. Yan et al. (1995) and Moisan and Niiler (1998) found considerable sensitivity to their results in the North Pacific to the depth of integration, with the best results found in comparisons with surface flux for an integration to the depth of a fixed isotherm about 1°C colder than the coldest surface temperatures, which they refer to as the "wintertime ventilation isotherm." Surface fluxes are balanced by ocean heat content changes through efficient vertical mixing; however, many other processes are neglected. For example, horizontal transport of heat and large vertical motion across the thermocline can considerably complicate the mixed layer budget. The analysis here therefore attempts a more complete budget analysis using physical constraints to infer divergences.

We use adjusted TOA radiation from the Earth Radiation Budget Experiment (ERBE) (Barkstrom and Hall 1982), for February 1985–April 1989, and the Clouds and Earth's Radiant Energy System (CERES) (Wielicki et al. 1996), for March 2000–May 2004, retrievals, along with comprehensive estimates of the divergence of the vertically integrated atmospheric energy components, computed from both National Centers for Environmental Prediction–National Center for Atmospheric Research (NCEP–NCAR) reanalysis (NRA; Kistler et al. 2001) and 40-yr European Centre for Medium-Range Weather Forecasts (ECMWF) ReAnalysis (ERA-40; Uppala et al. 2005). The annual cycle of the TOA radiation fluxes and atmospheric energy transports and divergences are given in Trenberth and Stepaniak (2003a,b, 2004). Here, F_S is computed as

a residual that allows the implied annual mean $\nabla \cdot \mathbf{F}_O$ to be inferred. The transports derived from this method have been shown to correspond quite well with direct observations from ocean hydrographic sections (Trenberth and Caron 2001).

Here we examine the annual cycle of F_S and compare it with direct observations of O_E from three sources, including *WOA 2005* (Locarnini et al. 2006), the analysis of the Japanese Meteorological Association version 6.2 (JMA; Ishii et al. 2006), and the Global Ocean Data Assimilation System (GODAS; Behringer and Xue 2004; Behringer 2007). We analyze the overall ocean energy budget and its agreement with fundamental global constraints in a range of estimates. We conclude that many of the results are dominated by physically real changes, thereby revealing new aspects of the annual cycle of ocean energy divergence. Nevertheless, residual errors are significant in instances, and their influence is quantified. Section 2 describes the data and the processing, section 3 presents the results, and section 4 discusses the results and their implications; conclusions are drawn in section 5.

2. Data and methods

A more detailed discussion of the datasets and methods is given in Fasullo and Trenberth (2008a, hereafter FT08). We use a prime to denote a departure from the annual mean. Figure 1 illustrates the relationships outlined in the equations below.

a. Energy budgets

The dominant energy terms and balances for the vertically integrated atmosphere and ocean are presented briefly below. In the atmosphere,

$$F_S = \nabla \cdot \mathbf{F}_A + \partial A_E/\partial t - R_T, \tag{1}$$

where F_S and R_T have been previously defined, and $\nabla \cdot \mathbf{F}_A$ and $\partial A_E/\partial t$ are the vertically integrated atmospheric total energy divergence and tendency, respectively. Moreover, for the ocean, given F_S and O_E, the divergence of ocean energy transport can be inferred based on

$$\nabla \cdot \mathbf{F}_O + F_S + \partial O_E/\partial t = 0, \tag{2}$$

and the ocean energy is approximated by the ocean heat content,

$$O_E = \int T(z)\rho C_w \, dz, \tag{3}$$

where z is depth, ρ is water density, T is the ocean temperature, and C_w is the specific heat of seawater. The challenges in diagnosing the terms in (1)–(3) include obtaining high-quality analyses of global observations with adequate sampling of the large temporal and spatial gradients of all terms.

b. Adjusted satellite retrievals

For terms in the TOA budget contributing to R_T, adjusted satellite retrievals from ERBE (February 1985–April 1989; Barkstrom and Hall 1982; FT08) and CERES (March 2000–May 2004; Wielicki et al. 1996; FT08) are used. While the ERBE retrievals offer multisatellite sampling, the CERES data show lower noise, improved ties to ground calibration, and smaller fields of view than ERBE (Loeb et al. 2007). CERES instrument calibration stability on *Terra* is claimed to be typically better than 0.2%, and calibration consistency from ground to space is better than 0.25%. Because both the ERBE and CERES estimates are known to contain spurious imbalances, however (Trenberth 1997; Wielicki et al. 2006), adjustments are required, as described in FT08, such that estimates of the global imbalance during the ERBE and CERES periods (Hansen et al. 2005; Willis et al. 2004; Huang 2006; Levitus et al. 2005) are matched. Associated uncertainty estimates, equal to two sample standard deviations of interannual variability ($\pm 2\sigma$), are reported here to quantify the uncertainty associated with the limited ERBE and CERES time periods. For all analysis here these adjusted ERBE and CERES fields are thus used, and in no instances are the raw fields used.

c. Reanalysis datasets

To solve for F_S from (2), estimates of the atmospheric tendency and divergence are required, except for the global average where divergence is zero by definition. In constructing estimates of these terms we use only fields strongly influenced by observations, such as surface pressure and atmospheric temperature and humidity from NRA and ERA-40. Estimates of the monthly mean vertically integrated storage, transports, and divergence of energy within the atmosphere for ERA-40 and NRA were computed and evaluated as in Trenberth et al. (2001), and for NRA these estimates have been updated through 2006 (additional information available online at http://www.cgd.ucar.edu/cas/catalog/newbudgets; see also Trenberth and Stepaniak 2003a,b; FT08). However, because ERA-40 fields are not available beyond 2001, the ERBE period is the primary focus of the present study.

d. Ocean surface fluxes and storage

The computation of F_S as a residual is superior to both model-based and Comprehensive Ocean Atmosphere Dataset (COADS) surface fluxes in terms of

biases, because the latter both suffer from systematic biases and fail to satisfy global constraints (Trenberth et al. 2001). Grist and Josey (2003) wrestled with how to best adjust their COADS-based estimates to satisfy energy transport constraints, suggesting adjustments to the fluxes and the need for further refinements associated with clouds. Trenberth and Caron (2001) used the long-term annual means of F_S during the ERBE period to compute the implied meridional ocean energy transports. Results agreed quite well with independent estimates from direct ocean measurements within the error bars of each in numerous sections. Moreover, they are reasonably compatible with estimates from state-of-the-art coupled climate models. However, the annual mean F_S (Trenberth et al. 2001; Trenberth and Stepaniak 2004) likely has various problems, especially over the southern oceans (Trenberth and Caron 2001).

The ocean datasets used to diagnose ocean heat content include the *WOA 2005*, JMA, and recently corrected (6 February 2006) GODAS. While some insight into the likely biases of O_E from these data can be gained from their degree of closure with F_S (FT08), uncertainty in the observations, and particularly the decomposition of error into its systematic and random components, has been hampered by a lack of observations, particularly at depth. Here we also use departures from this mean for the ERBE period and thus gain the advantage of subtracting out most systematic errors or biases. Estimates of F_S over the ocean are based on (2), and their accuracy is of the order of 20 W m^{-2} over 1000-km scales while satisfying closure among F_S, $\nabla \cdot \mathbf{F}_A$, $\delta A_E/\delta t$, and R_T (Trenberth et al. 2001). A cancellation of errors in $\nabla \cdot \mathbf{F}_A$ occurs over larger scales because divergence is zero globally by definition. Uncertainty in F_S is governed mainly by the uncertainties in R_T and $\nabla \cdot \mathbf{F}_A$. By exploiting the constraint that F_S and $\partial O_E/\partial t$ must balance globally, FT08 identify an excessive annual cycle of O_E in JMA and *WOA* relative to that which can be explained by either a broad range of F_S estimates or GODAS fields.

In estimating ocean heat from (3), we essentially follow the calculations of Antonov et al. (2004). However, therein the density of seawater (ρ) was assumed to be 1020 kg m^{-3} and the specific heat (C_w) was assumed to be 4187 J kg^{-1} K^{-1}, whereas for the typical salinity of the ocean of ~35 PSU, ρ is ~1025–1028 kg m^{-3} and C_w is 3985–3995 J kg^{-1} K^{-1} for temperatures from 2° to 20°C. The product ρC_w is more nearly constant than either of the two components, but the Antonov et al. value is 4.4% too high, leading to an overestimate of O_E and its annual cycle. Therefore, we have adjusted these constants and performed our own integration, using ocean temperatures provided at multiple levels in the *WOA*, where the depth of each layer is assumed to extend between the midpoints of each level. In the case of the surface, the layer is assumed to begin at 0 m and at 250 m-depth the layer is assumed to terminate at 275 m, half way to the next *WOA* layer at 300 m. We assign the density of ocean water at 1026.5 kg m^{-3} and specific heat at 3990 J kg^{-1} K^{-1}, although it is their product that determines O_E per (3).

Obvious spurious values of ocean heat content south of 20°S are edited out by accepting only the monthly departures from the annual mean within two standard deviations of the zonal ocean mean to take advantage of the lack of land over the southern oceans. Globally, the data are also filtered temporally by retaining the first three harmonics of the annual cycle. Oceanic energy tendencies are then computed by reassembling the Fourier series and differencing O_E between the start and end days of each month. Other small systematic differences may arise from methods of compiling the vertical integral and numerical aspects in computing O_E [which are not described by Antonov et al. (2004)]; however, tests show that the magnitude of the annual cycle is not significantly affected by these refinements. In general, the patterns of O_E derived here are quite similar to the actual O_E of Antonov et al. (2004) outside of the tropics, except the latter are ~10%–20% larger. One source of discrepancy can be the depth of integration, and Levitus and Antonov (1997) show that depths below 150 m are often somewhat out of phase with near-surface values. Deser et al. (1999) show how decadal changes in the Kuroshio Extension are associated with temperature changes exceeding 1°C in the main thermocline from 300- to 1000-m depth, and that such changes can occur in association with subduction and ventilation of the thermocline. However, integrating to greater depth brings in regions of fewer data and thus increases errors and noise, and we therefore limit the depth of integration to 275 m. This may lead to errors in the annual cycle, although the phasing with depth affects whether it amplifies or diminishes the annual cycle. Analysis of fields integrated to 500 m shows results that are fundamentally unchanged from the results presented here.

e. Regridding and standard deviations

To provide a consistent delineation of land–sea boundaries among the datasets, all fields are transformed to a grid containing 192 evenly spaced longitudinal grid points and 96 Gaussian-spaced latitudinal grid points using bilinear interpolation (i.e., to a T63 grid). Spatial integrals are calculated using Gaussian weights over the T63 grid and a common land–sea mask is applied. Total energy is expressed in units of peta-

watts (PW = 10^{15} W) and monthly mean values are used for all calculations. In quantifying seasonality, the estimated population standard deviation of monthly values is used.

f. Secondary terms

Within the ocean, the formation and melting of sea ice can influence O_E. An estimate of this effect from the latent heat of fusion can be obtained from estimates of the annual cycle in ice volume from an ice model by Köberle and Gerdes (2003) for the Arctic, driven by NRA atmospheric fields, of about 1.5–3.2 $\times$ 10^4 km^3, which is also broadly consistent with energy budget estimates of Serreze et al. (2006, 2007). These studies thus suggest a heating amplitude of 0.5 PW for the annual cycle's first harmonic. Moreover, the transport of water vapor to land and its storage as either snow or water affects the mass of the ocean and sea level (Minster et al.1999) and is associated with an energy flux estimated near 0.1 PW (FT08). For global budgets, it is expected that some degree of compensation between sea ice formation in the Antarctic balances that in the Arctic; however, reliable estimates of the net global budget remain unavailable. Nevertheless, this initial scale comparison suggests that overall the global imbalance at TOA should be reflected primarily in O_E (Levitus et al. 2005).

3. Results

a. The annual mean F_S

The annual mean F_S based on ERBE–NRA residuals is shown in Fig. 2a, with stippled and hatched regions highlighting the regions of difference with ERA-40-based estimates exceeding $\pm$10 W m^{-2}. For both estimates, the tropics exist as a region of strong energy flux into the ocean ($F_S < 0$), particularly in the eastern Pacific Ocean. In contrast, the subtropics, where evaporative cooling is strong (Trenberth and Stepaniak 2004), and high latitudes are characterized by strong ocean cooling in the annual mean ($F_S > 0$). Zonal gradients in F_S are large in the midlatitudes, with particularly strong ocean cooling in the western boundary currents (e.g., Gulf Stream, Kuroshio) and generally modest ocean warming in the eastern basins. The values in the Southern Hemisphere (SH) midlatitudes are smaller and more zonally symmetric than in the Northern Hemisphere (NH). Key differences (Fig. 2a) are found both in the tropics and SH midlatitudes, where $\nabla \cdot \mathbf{F}_A$, and thus F_S, in ERA-40 exceed NRA, and through much of the subtropics, where ERA-40 estimates of $\nabla \cdot \mathbf{F}_A$, and F_S are less than those of NRA. We

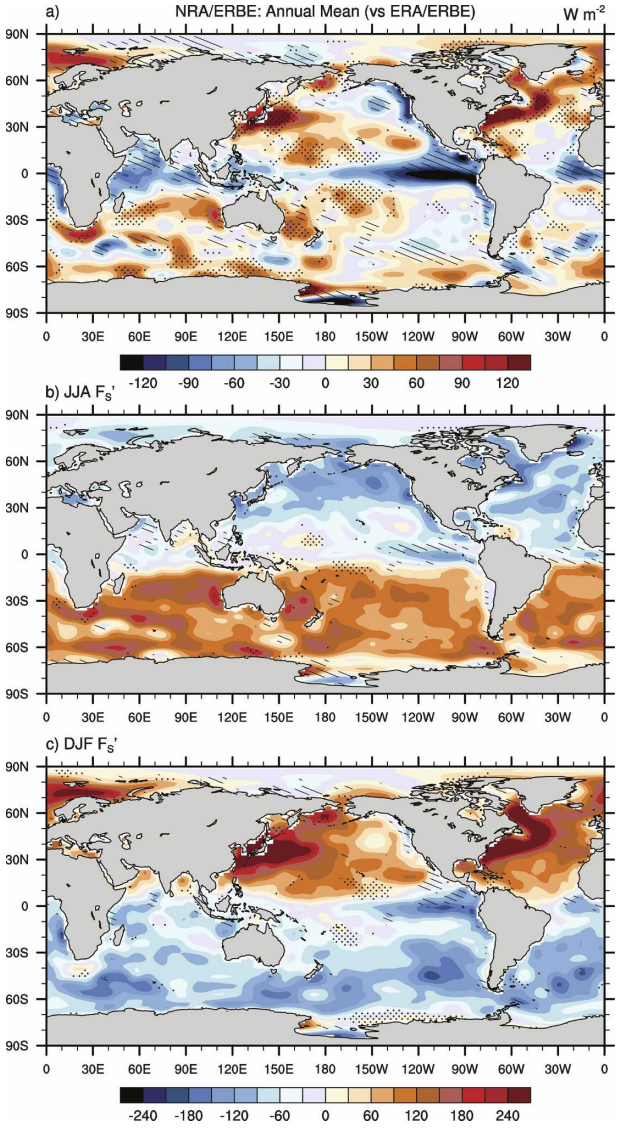

FIG. 2. (a) Annual mean F_S as computed by the residual from R_T and NRA atmospheric energy budgets for the ERBE period (W m^{-2}). Departure from the annual mean of the (b) JJA and (c) DJF surface flux out of the ocean (W m^{-2}). Stippling (hatching) denotes areas where NRA-based estimates exceed (fall below) those of ERA-40 by more than 10 W m^{-2} in (a) and by more than 30 W m^{-2} in (b) and (c).

have not performed comparisons with in situ surface flux estimates because there are global biases of several tens of watts per squared meter in unconstrained voluntary observing ship observation-based products (Grist and Josey 2003).

b. The annual cycle

Figure 3 presents the annual cycle of two of the dominant contributors to F_S, namely, R_T and $\nabla \cdot \mathbf{F}_A$ ($\delta A_E/\delta t$

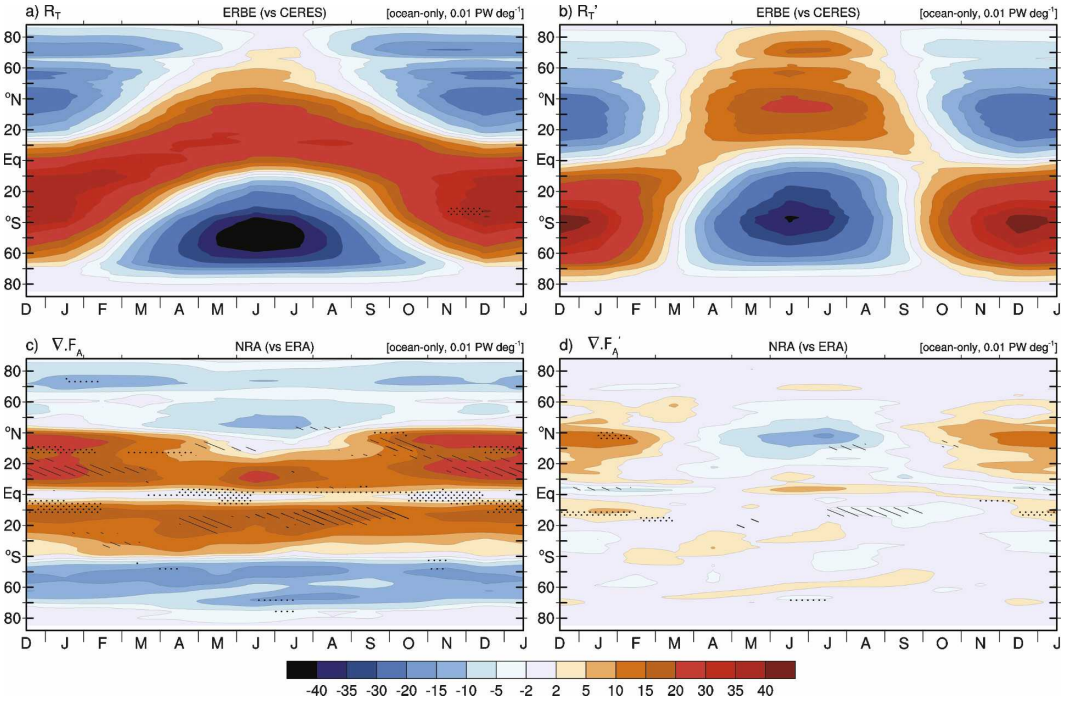

FIG. 3. Zonal mean of the (left) total and (right) departure from the annual mean for the (top) incoming radiation at the TOA and (bottom) the column-integrated atmospheric energy divergence over the oceans in 0.01 PW deg^{-1} for the ERBE period. Stippling (hatching) denotes areas where ERBE and NRA-based estimates exceed (fall below) those of CERES and ERA-40 by more than 0.02 PW deg^{-1}.

is relatively small). The zonal mean is averaged over the oceans only and both the total and the departure from the annual mean are presented. A distinct annual cycle is evident in $\nabla \cdot \mathbf{F}_A$ in the NH as energy is transported in winter from ocean to land, where it is mostly radiated to space (FT08). The reverse occurs in summer, though to a lesser extent than during winter, when high temperatures from midlatitude land contribute to the divergence of energy to ocean regions. However, in the SH the lack of significant extratropical land extent results in a steady pattern of poleward energy transport with few zonal asymmetries, and the annual cycle of $\nabla \cdot \mathbf{F}_A$ is very small (Fig. 3d).

The zonal means in Fig. 3 integrate over large domains and thus mask the strong zonal structure of F_S; see Figs. 2b,c for June–August (JJA) and December–February (DJF) F_S departures from the annual mean with stippling and hatching for differences with ERBE–ERA-40 estimates of ± 30 W m^{-2}. The solstitial season F_S fields are dominated by the change in net surface solar radiative flux, and hence the large negative values in summer designate energy flux into the ocean and contrast with the positive values that are pervasive in the winter hemisphere. Some finer-scale structures correspond to components of the ocean circulation. In NH winter (Fig. 2c) the largest values of annual mean departures of F_S off the east coasts of the major continents exceed 240 W m^{-2} and arise as cold, dry air is advected off the continents over the warm Gulf Stream and the Kuroshio, resulting in large sensible and latent heat fluxes into the atmosphere and corresponding maxima in atmospheric energy divergence (Fig. 3d) (e.g., Bunker 1976). The lack of analogous features in F_S in summer highlights the skewed influence of the boundary currents toward winter and contributes to their rectified impact on the annual mean fluxes, which exceed 140 W m^{-2} in western boundary regions (Fig. 2a), so that the total winter fluxes exceed 360 W m^{-2} in these regions. In contrast, both the annual mean and seasonal extreme fluxes are much weaker in the eastern North Pacific, North Atlantic, and SH oceans. In the tropics, seasonal contrasts are less than in midlatitudes, and F_S is positive in the primary upwelling zones for both solstitial seasons.

The mean annual cycle of F_S zonally averaged over the oceans (Fig. 4a), which is represented by the difference between Figs. 3b,d, features peak solstice values in both hemispheres, with maxima exceeding 0.3 PW deg^{-1}. (Note that zonal means are expressed as integrals rather than averages to better depict the meridional structure. Rather than use per meter as the remaining dimension, we have chosen to use 1° latitude,

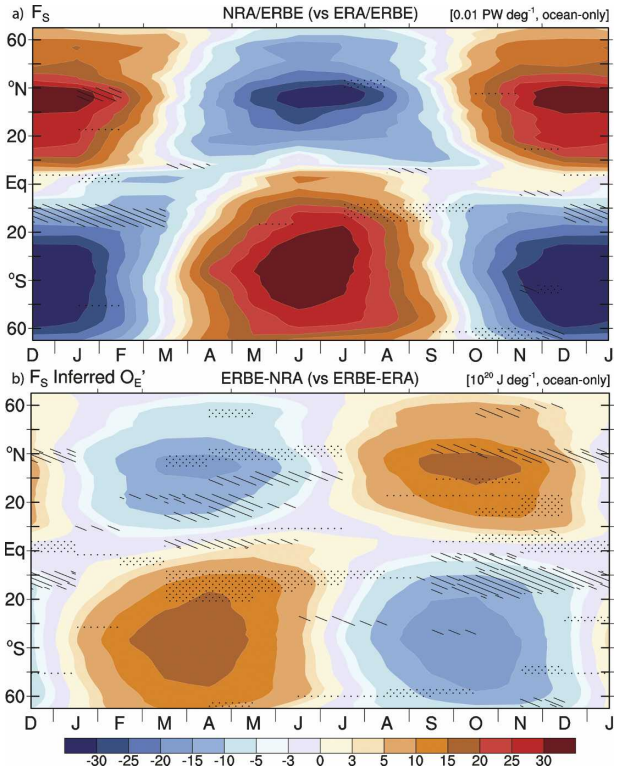

FIG. 4. Zonal mean over the world's oceans of the departure from the annual mean of the (a) net surface flux out of the ocean in 0.01 PW deg^{-1}. Stippling (hatching) denotes areas where NRA-based estimates exceed (fall below) those of ERA-40 by more than 0.02 PW deg^{-1}. (b) The vertically integrated equivalent O_E in 10^{20} J deg^{-1} corresponding to Fig. 3a. Stippling (hatching) denotes areas where NRA-based estimates exceed (fall below) those of ERA-40 by 5×10^{19} J deg^{-1}.

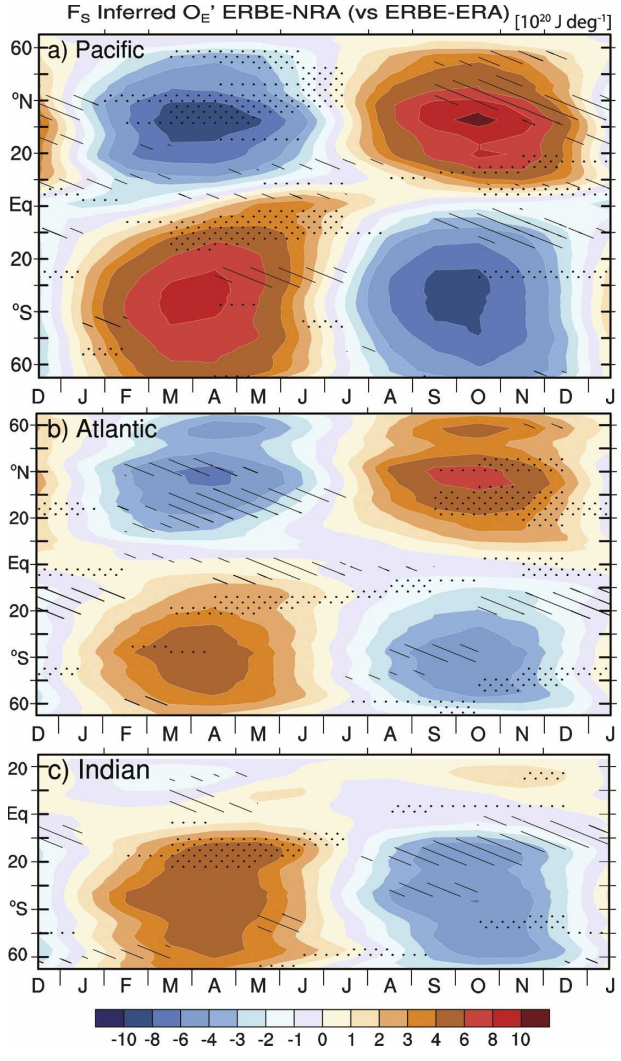

FIG. 5. Zonal mean of the annual cycle of equivalent O_E in 10^{20} J deg^{-1} for the (a) Pacific, (b) Atlantic, and (c) Indian Oceans. Stippling (hatching) denotes areas where NRA-based estimates exceed (fall below) those of ERA-40 by 2.5×10^{19} J deg^{-1}.

as 111.3 km. Thus, the units are petawatts per degree.) From approximately 5°S to 10°N a semiannual oscillation peaks positively in May through July and November through December, and negatively in January through March and September through October. Uncertainty in F_S is greatest in the tropics and high latitudes, where estimates of $\nabla \cdot \mathbf{F}_O$ and F_S in ERA-40 are larger than in NRA, and in the subtropics, where ERA-40 estimates are less than those of NRA.

Integration of F_S in time provides an estimate of the annual cycle of equivalent O_E (Fig. 4b) in 10^{20} J deg^{-1} latitude for comparison with direct calculations of O_E (Antonov et al. 2004). Upper-ocean energy content for the Pacific, Atlantic, and Indian Oceans (Fig. 5) can be similarly compared. In general, the patterns of equivalent O_E are quite similar to the O_E values of Antonov et al. (2004) outside of the tropics, except that the latter are ~10%–20% larger, even with the corrected physical constants. Differences in equivalent O_E values derived from F_S based on ERA-40 and NRA fields are associated primarily with differences in the meridional structure of $\nabla \cdot \mathbf{F}_A$ (Fig. 3d). For the seasonal cycle, these differences translate to smaller (larger) equivalent O_E in the north (south) equatorial ocean from March to June and larger (smaller) equivalent O_E from October through December in NRA-based estimates relative to ERA-40-based estimates; differences are evident in all three ocean basins (Fig. 5).

The zonal mean $\delta O_E/\delta t$ from GODAS, its differences with *WOA*, and the implied $\nabla \cdot \mathbf{F}_O$ based on (2) are given in Fig. 6. The general pattern of change in O_E is quite similar to that of F_S (Fig. 4a) in the extratropics, with peak values occurring at the solstices. However, $\delta O_E/\delta t$ exceeds F_S in the midlatitudes by an order of 0.01 PW deg^{-1} in both hemispheres. If real (discussed

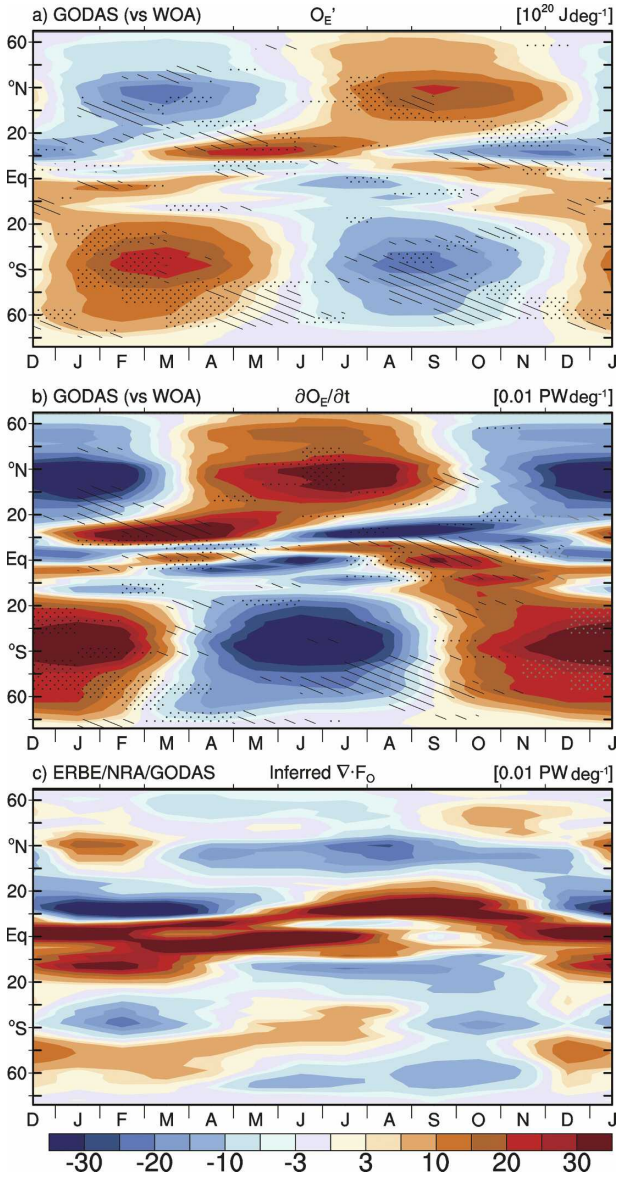

FIG. 6. Zonal integral over the world's oceans of (a) O_E' (10^{20} J deg^{-1}), (b) $\delta O_E/\delta t$ (0.01 PW deg^{-1}), and (c) inferred $\nabla \cdot \mathbf{F}_O$ (0.01 PW deg^{-1}). Hatching (stippling) in (a) corresponds to instances in which *WOA* values of monthly values of $\delta O_E/\delta t$ exceed (fall below) those of *WOA* by 0.03 PW deg^{-1}, or 10^{20} J deg^{-1} for O_E'.

later), this difference is related to the transport of heat (Fig. 6b) between the middle and lower latitudes, because areal extent at high latitudes is relatively small. The strong meridional structure in the seasonal cycle of $\nabla \cdot \mathbf{F}_O$ (Fig. 6b) consists of divergence maxima in the tropics and summer subtropics that exceed those at midlatitudes, and convergence maxima in subtropical winter subtropics and summer midlatitudes. The complexity of the annual cycle in $\delta O_E/\delta t$ between 15°S and 20°N is not reflected in F_S, and thus the key role of tropical ocean current variations and their effects on $\nabla \cdot \mathbf{F}_O$ in the mixed layer energy budget are indicated. As shown later, the exchanges are likely related mainly to Ekman transports. Discrepancies between GODAS and *WOA* estimates are widespread in SH winter and have been associated with the lack of observations in austral winter (Fasullo and Trenberth 2008b). The principal features of Fig. 6b are robust in the context of uncertainties in $\nabla \cdot \mathbf{F}_O$, which are quantified later (Fig. 11).

c. Joint EOF analysis

To identify variability in the spatially and temporally complex fields of $\nabla \cdot \mathbf{F}_O$, a joint EOF analysis is performed that combines the F_S and $\delta O_E/\delta t$ fields and extracts common modes of variability. The first extended joint EOF (Fig. 7) gives the dominant annual cycle and accounts for 63% of the combined variance. The second EOF (not shown), which accounts for 12% of the variance, has a semiannual time series with peaks in April and October–November, and minima in July and January–February. It is dominated by O_E changes in the tropics, particularly the Indian Ocean, and is not primarily related to F_S. We therefore focus here only on the first EOF. In Fig. 7 both the EOF pattern and the principal component time series are rescaled (their product is what matters physically) so that the latter has a maximum value of unity, and thus the EOF values can be interpreted reasonably well in terms of watts per squared meter. The patterns in the top two panels (Fig. 7) are somewhat similar in the extratropics, with the amplitude of $\delta O_E/\delta t$ larger by an order of 50 W m^{-2}. The associated $\nabla \cdot \mathbf{F}_O$ (Fig. 7c) is tightly tied with F_S and $\delta O_E/\delta t$ at mid- and high latitudes. In the tropics, the mode strongly resembles the spatial structure and seasonal coherence of the intertropical convergence zone.

The zonal mean of EOF1 of $\nabla \cdot \mathbf{F}_O$ (Fig. 8a) features strong divergence in the summer subtropics, and convergence in winter, that are balanced by variability in the tropics and midlatitudes and by cross-equatorial transports. The annual cycle in midlatitude O_E is thus enhanced by $\nabla \cdot \mathbf{F}_O$ over that expected from F_S alone by over 0.09 PW deg^{-1} in the NH and 0.06 PW deg^{-1} in the SH. Moreover, the seasonal phase is quite uniform between hemispheres in time, and its spatial structure differs from that of F_S, with maxima in the tropics and subtropics, particularly north of the equator, and in the fine meridional structure near the equator. The primary coherent contributions in EOF1 arise from spatial coherence across the subtropics (8°–30°N and 5°–29°S), with midlatitude and tropical peaks of opposite signs but weaker magnitudes, which together compensate for the subtropical variability.

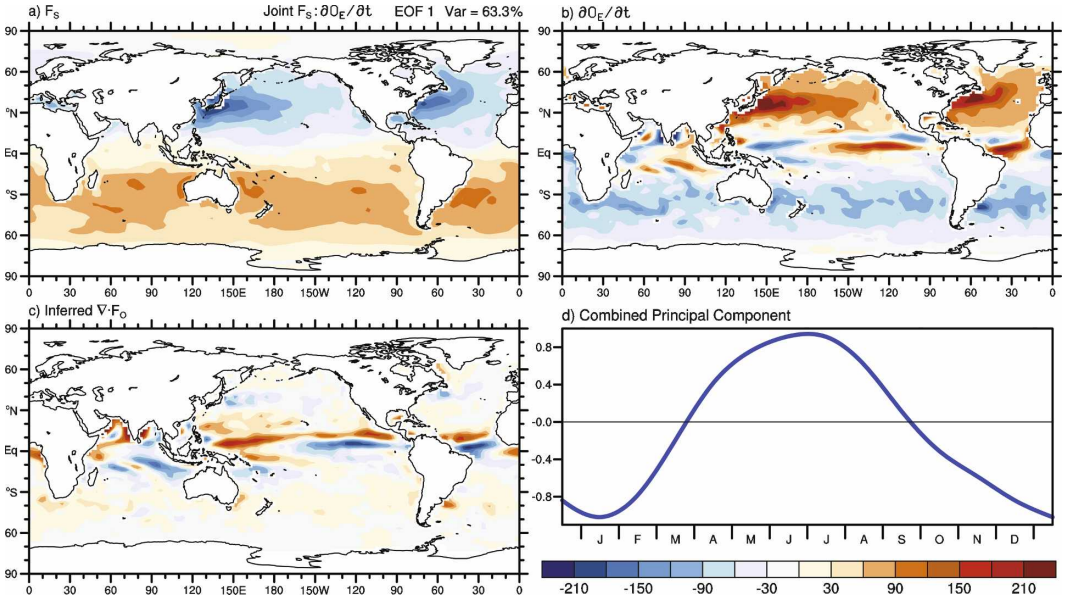

FIG. 7. First EOF of the combined extended EOF analysis for F_S and O_E plus their principal component time series: (a) F_S, (b) $\delta O_E/\delta t$, and (c) the inferred $\nabla \cdot \mathbf{F}_O$ from (2). (d) The principal component time series is scaled to have extremes of ± 1, so that the EOFs approximately depict units of W m^{-2}.

d. Principal balances in EOF1

Integrating Fig. 8a over regions of coherent variability clarifies the basic energy exchanges associated with $\nabla \cdot \mathbf{F}_O$. Because the integral from 65°N to 65°S yields cancellation during all months (Fig. 8c), and thus satisfies the fundamental global constraint of zero net divergence on its own, the linear approach is adopted. In the NH (Fig. 8a,b), the principal balance in $\nabla \cdot \mathbf{F}_O$ is between the northern tropics and subtropics (8°–30°N) and the nearly equal contributions from a portion of the deep tropics (2°S–8°N) and midlatitudes (30°–65°N). The net magnitude of the implied exchange is $\sim \pm 2.2$ PW. A residual NH energy transport of $\sim \pm 0.6$ PW occurs in phase with the subtropical domain.

In the SH, compensation between the southern tropics and subtropics (2°–29°S) is largely balanced by variability in midlatitudes that is ~70% stronger than in the NH, with the subtropical contribution exhibiting a magnitude of ± 3.7 PW. An equal and opposite residual transport is also evident from the 2°–65°S integral that is in phase with the southern subtropical contribution and balances that from the NH.

e. Implied meridional transports

From the derived fields of $\nabla \cdot \mathbf{F}_O$, we estimate the ocean's integrated meridional transport (Fig. 9) and its associated uncertainty, both for the zonal mean annual cycle (Fig. 9a) and the zonal annual mean, both globally and for individual ocean basins (Fig. 9b). There are nine estimates considered in Fig. 9, associated with each permutation of the three estimates of F_S and $\delta O_E/\delta t$. Also shown in Fig. 9b are the mean values obtained from numerous ocean sections. The annual cycle of transport is significant in the tropics and subtropics, and transports are strongest in the winter hemisphere.

In winter, poleward transports exceed 4 PW from November through April in the NH, and 3 PW from June through October in the SH. Thus, the seasonal minimum identified by Zhang et al. (2002) at 24°N in February is an exception for NH winter, where northward transports are otherwise strong and positive. There is often a broad, coherent meridional scale for the estimated transports. For example, in southern winter, southward transports extend from 15°N to 60°S with a substantial cross-equatorial flux that exceeds 4 PW in September. Perhaps more surprising is the broad meridional scale of northward transports during December, at which time global ocean transports are northward throughout most of the SH (to 50°S) and cross-equatorial transports again exceed 4 PW. From April to September, the poleward transports of heat in the SH coincide with reductions in ocean heat content (from May to October; Fig. 6), and hence mostly help feed surface energy fluxes into the atmosphere, especially in the tropics and subtropics.

A key to understanding the relationship between divergence and transports is the summer tropical to subtropical divergence maxima, which contribute substantially to the winter poleward transport and cross-

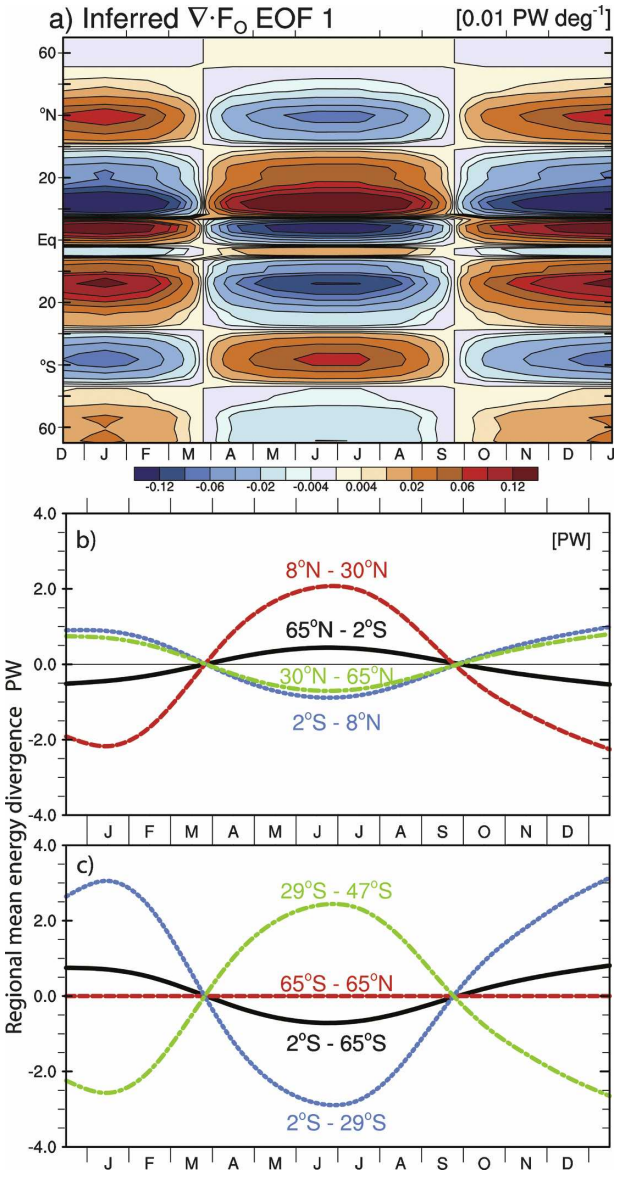

FIG. 8. (a) The zonal mean of the implied $\nabla \cdot \mathbf{F}_O$ from Fig. 6c for the annual cycle (0.01 PW deg^{-1}). (b), (c) Regional integrals of $\nabla \cdot \mathbf{F}_O$ EOF1 (Figs. 6c, 7a) for zones as labeled in PW. Zones are chosen to isolate the main regions of coherence from Fig. 7a and to illustrate fundamental balances.

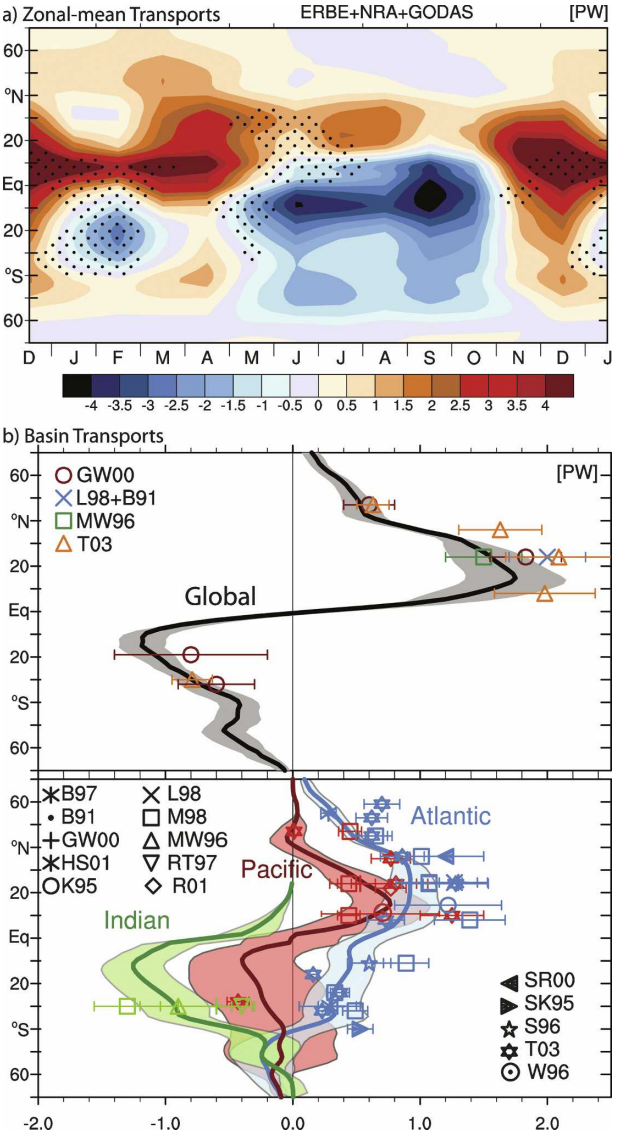

FIG. 9. Integrated meridional ocean heat transports in PW and their uncertainty for the (a) zonal mean annual cycle, (b) zonal annual global mean and zonal ocean basin means. Stippling in (a) represents the regions and times of the year in which two std dev of monthly mean values among estimates, some of which include the CERES period (see text), exceed 0.5 PW. Transport in (b) is the median annual mean transport by latitude from all estimates and the associated $\pm 2\sigma$ range (shaded). Observational estimates include Bacon (1997): B97, Bryden et al. (1991): B91, Ganachaud and Wunsch (2000): GW00, Holfort and Siedler (2001): HS01, Klein et al. (1995): K95, Lavin et al. (1998): L98, Macdonald (1998): M98, Macdonald and Wunsch (1996): MW96, Robbins and Toole (1997): RT97, Roemmich et al. (2001): R01, Sato and Rossby (2000): SR00, Saunders and King (1995): SK95, Speer et al. (1996): S96, Talley (2003): T03, and Wijffels et al. (1996): W96.

equatorial transports in some months. The importance of higher-order modes is underscored, because a large portion of the transport is not accounted for by EOF1 (Fig. 8). Uncertainty in the annual cycle of transport, estimated by two standard deviations (2σ) of the estimates of transport included in Fig. 9, exceeds 0.5 PW in the tropics and subtropics during much of the year and is greater than 1.0 PW from December through February in the tropics and SH subtropics and from April through July in the tropics and subtropics (not shown).

The annual zonal mean structure of transport is characterized by a northward maximum at 15°N of 1.7 $\pm$0.3 PW, and a southward maximum at 11°S of 1.2 $\pm$0.5 PW where the uncertainty is $\pm 2\sigma$. A steep meridional gradient in transport in the deep tropics reflects the strong

net energy flux into the ocean on the equator (Fig. 2). Despite the pronounced seasonal variability in cross-equatorial transports (Fig. 9a), the annual mean cross-equatorial transport is negligible (<0.1 PW), with an upper $\pm 2\sigma$ bound of 0.6 PW.

The structure of global annual mean transports is generally supported by observed oceanographic sections (Fig. 9), with close agreement at 47°N and 30°S and agreement within the range of uncertainty at 24°N, 8°N, and 20°S. At 36°N, the observed estimate of Talley (2003) exceeds the values derived here by about 0.6 PW, which lies beyond the 20% (0.3 PW) error range provided by Talley. Our NH northward transports are systematically less than the ocean estimates between 0° and 40°N, and this bias occurs in the North Atlantic.

Mean transport in the Atlantic Ocean is northward north of 40°S, while in the Indian Ocean, it is southward at all latitudes. In the Pacific Ocean, transport is positive in the NH and negative in the SH. As in Trenberth and Caron (2001), the magnitude of mean transports is comparable among the basins, with a southward peak of 0.8 PW at 12°S in the Indian Ocean, a northward peak of 0.8 PW at 40°N in the Atlantic Ocean, and northward and southward peaks of 0.9 PW at 13°N and 0.6 PW at 10°S, respectively, in the Pacific Ocean.

In the Atlantic, agreement with some direct ocean estimates is good, including those of Bacon (1997) at 47°N, Speer et al. (1996) at 36°N, and Talley (2003) at 8°N and 18°S. In other instances, disagreement between the estimates is large, such as for Talley (2003) at 47°N, Macdonald (1998) at 8°N, and Speer et al. (1996) and Macdonald at 8°S, although in several of these cases there are also disagreements among the direct ocean estimates that are outside the estimated error bars. Agreement with observed sections in the Pacific is good for Talley (2003) at 47°N and numerous estimates at 30°N, and for both the Indian and Pacific basins at 30°S. At 10°N in the Pacific the two direct estimates of Macdonald (1998) and Talley (2003) are at odds and our value is in between. Uncertainty in transports, based on the range of estimates derived herein, is largest in the Indian Ocean, where sampling of the upper ocean is sparse (Locarnini et al. 2006), variability in F_S is large, and the heat budget of the upper ocean is complex (Loschnigg and Webster 2000).

4. Discussion

While agreement between estimates of transport derived herein and those from ocean sections are reassuring, there is considerable uncertainty in both (e.g., Bryden et al. 2005). Additionally, temporal sampling is an issue (Koltermann et al. 1999), as indicated, for instance, by the variability of Florida Strait cable estimates of current transports (Baringer and Larsen 2001) and recent moored measurements at 26.5°N (Cunningham et al. 2007). Many direct ocean estimates are biased toward spring and summertime. Similarly, instances in which disagreement between the estimates are large does not preclude the validity of our analysis. Moreover, in some regions, such as in the tropical Pacific and northern Atlantic Oceans, the observations themselves are mutually inconsistent. In many instances where the observations are at odds, the transports provided herein represent a reasonable compromise between the direct observed values. Hence, the current analysis represents an important additional basis for assessing ocean energy transports.

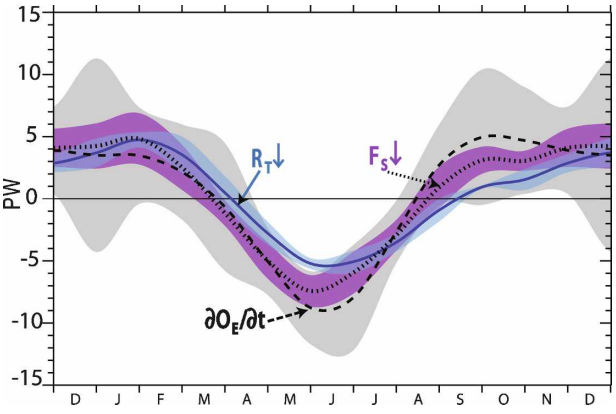

FIG. 10. Global mean annual cycles for the ERBE period of R_T (solid blue), F_S over ocean (dots–purple), and GODAS $\delta O_E/\delta t$ (dashes–gray) in PW. Shading represents σ of monthly means for each field.

a. Consistency of results: Global constraints

Here we briefly explore the robustness of our findings based on global constraints (Fig. 10), a topic dealt with in more detail by FT08. TOA solar energy coming into the earth system is a maximum on 3 January at the time of perihelion, with annual cycle amplitude of 3.4%. However, the net global R_T peaks in February at 4.5 PW, because the lower albedo mainly from clouds in February comes into play along with the annual minimum of outgoing longwave radiation. The minimum in R_T in June and July is ~ -5 PW. This imbalance in R_T should be reflected primarily in both F_S and O_E, because energy storage in the atmosphere and on land is small. The larger ocean area in the SH dominates the global ocean annual cycle, which in turn balances R_T. However, in the NH there is a major transport of energy from ocean to land in winter by atmospheric winds (see Fig. 3; FT08), so that the TOA radiation is not the

only driver of F_S over the oceans. Net evaporation over the oceans and transport of latent energy to land areas results in annual cycle variations in water (or snow and ice) on land and sea level, as observed by altimetry (Minster et al. 1999), with amplitude equivalent to 9.5 mm of sea level, peaking in September.

Globally, the difference between the TOA radiation and F_S over ocean (Fig. 10) arises primarily from the small contributions from land storage tendency (FT08). Some energy storage also occurs in sea ice as an energy deficit in winter that is released in summer, although presumably the energy tendency associated with sea ice largely cancels between the two hemispheres when integrated globally. Hence, F_S over ocean appears principally as a change in O_E. The ocean temperature datasets imply a larger annual cycle of O_E than F_S estimates do, and tendencies are outside the error bars in southern winter (too low) and October–November (too high) (Fig. 10), and correspond to O_E values that are too high in March–April and too low in August–October. In FT08 and Fasullo and Trenberth (2008b) it is shown that the errors most likely arise from O_E south of 40°S, where *WOA* and JMA values are further astray from GODAS, given in Fig. 10.

b. Ekman transports

The biggest differences between the results in Figs. 4 and 6 and those of Antonov et al. (2004) are in the tropics, notably from ~5° to 15°N, and especially in the Pacific where there is strong evidence for the annual cycle being dominated by ocean dynamics. The zero wind stress curl line over the North Pacific migrates from 11°N in March to 20°N in September and induces upper-layer thickness anomalies across the Pacific basin, resulting in major seasonal changes in the North Equatorial Current (NEC) and where it bifurcates along the western boundary. The NEC is farthest north in October and farthest south in February (Qiu and Lukas 1996). Furthermore, large seasonal changes in Ekman transports lead to a substantial annual cycle in northward energy transports throughout the tropics (Jayne and Marotzke 2001), and at 24°N (Zhang et al. 2002) range from about zero in winter to maxima in July and November of 1 PW.

In the Atlantic, the NEC peaks in boreal summer and weakens during spring and fall (Arnault, 1987). Böning and Herrmann (1994) present results for a North Atlantic Ocean model simulation and the annual cycles of surface fluxes and O_E show similar results to those presented here. In the Atlantic at 8°N they also find a large annual cycle in northward energy transports in which the strong NEC-induced changes in O_E have little to do with F_S, but depend rather on changes in surface stress. Kobayashi and Imasato (1998) determine that substantial annual cycles exist in meridional energy transports in the Atlantic and Pacific, with the largest values around 10°N. Seasonal variability in energy transport of 100% is also suggested for the Indonesian Throughflow, and in the Indian Ocean the annual cycle just south of the equator is suggested to be +1.4 PW in December through February and −1.8 PW in June through September (Loschnigg and Webster 2000). The regional results are consistent with the inferred fields presented here.

For the total meridional transport at 24°N, Zhang et al. (2002) estimate that the annual cycle ranges from 1.1 PW in February to 2.8 PW in August, with a mean of 2.1 ± 0.4 PW. The inference is that in both the Atlantic and Pacific transports enhance the annual cycle of O_E from what it would be based on F_S alone by about 10%, as was shown for the Atlantic in a model by Böning and Herrmann (1994). While the transports at 24°N from Zhang et al. (2002) are consistent with the fields derived here, albeit somewhat stronger, generally the behavior at 24°N is not representative of variability at other latitudes (Fig. 9), owing to the steep gradients in transport that exist in the subtropics seasonally and their complex relationship to cross-equatorial flow and midlatitude variability, which is relatively weak. Indeed, in model simulations, Jayne and Marotzke (2001) demonstrate the dominant role of the annual cycle in Ekman transports associated with broad overturning circulations in the tropics and subtropics that contribute to strong energy transport and underlie the deduced changes in O_E. Based on the surface forcing they use, Ekman transports reverse sign sharply at about 25° latitude in each hemisphere through the course of the annual cycle. Hence, the dipole structures seen in Figs. 7 and 8 near the tropics and midlatitudes in both hemispheres are qualitatively consistent with established changes resulting from Ekman transports. Moreover, the suitability of assessing these transports near the node of the overturning circulations, where the gradient in transport is strong, is called into question.

c. Factors contributing to uncertainty

Terms that contribute to uncertainty in $\nabla \cdot \mathbf{F}_O$ include contributions from 1) R_T (Fig. 11a) period fluxes, estimated from ERBE and both instruments on CERES; 2) the atmospheric budget (Fig. 11b), estimated from NRA and ERA-40 during ERBE and NRA during CERES; and 3) $\delta O_E/\delta t$ (Fig. 11c), estimated from the *WOA* climatology and JMA and GODAS fields during the 1990s. The estimated population standard deviation of zonal means for each term (Figs. 11a–c) and the zonal mean structure of uncer-

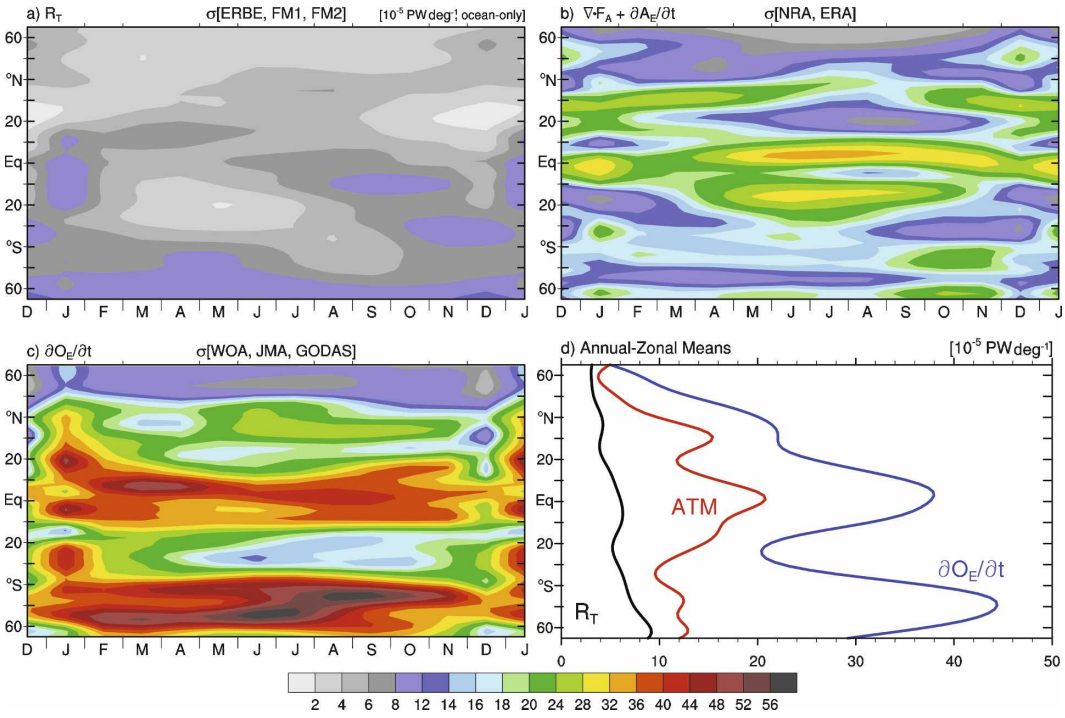

FIG. 11. Uncertainty analysis of terms contributing to estimation of $\nabla \cdot \mathbf{F}_O$, including (a) R_T, (b) $\nabla \cdot \mathbf{F}_O + dA_E/dt$, (c) $\delta O_E/\delta t$, and (d) the zonal means of the uncertainty in monthly means of each term (10^{-5} PW deg^{-1}). Estimates of uncertainty are based on the std dev among three estimates of each field, including (a) R_T derived from periods of ERBE and CERES (both instruments) fluxes, (b) estimates of $\nabla \cdot \mathbf{F}_O$ and $\delta A_E/\delta t$ taken from NRA and ERA-40 during ERBE, and NRA during CERES, and (c) estimates of $\delta O_E/\delta t$ from *WOA* fields, and from JMA and GODAS fields during the 1990s.

tainty in monthly means (Fig. 11d) are shown. The estimates are independent (e.g., ERBE and CERES fluxes are not used in the compilation of the reanalysis or ocean datasets), and there is no expectation that cancellation of uncertainty will occur when the fields are combined to infer $\nabla \cdot \mathbf{F}_O$. Because some of the differences between the fields in Fig. 11 represent real differences between the ERBE, CERES, and *WOA* time periods, the estimates (Fig. 11) somewhat overstate the analysis uncertainty. At TOA, uncertainty associated with R_T is largest in the SH but it is still small relative to other terms (less than 0.01 PW deg^{-1}). Uncertainty in $\nabla \cdot \mathbf{F}_A$, particularly in the tropics, is a substantial contributor to the uncertainty in $\nabla \cdot \mathbf{F}_O$, with values exceeding 0.05 PW deg^{-1} from March through November. Uncertainty associated with both the atmospheric budget and ocean tendencies is large in the subtropics, but near the node of EOF1 (Fig. 8) uncertainty returns to a relative minimum. In midlatitudes, large uncertainty is associated primarily with disagreements in estimates in the ocean tendencies; however, it decreases toward the poles. In the extratropics, where the moisture-holding capacity of the atmosphere is greatly reduced from that of the tropics, agreement between ERA-40 and NRA estimates of $\nabla \cdot \mathbf{F}_A$ is better and uncertainty is reduced. For the ocean, uncertainty associated with $\delta O_E/\delta t$ is greatest in SH mid- to high latitudes and is likely to be associated with the lack of observations, and hence the reliance on infilling techniques used in constructing ocean analyses in these regions. Because the overall trend in ocean temperatures is small across the 1990s, the annual zonal mean of $\delta O_E/\delta t$ is small compared to the other terms (Fasullo and Trenberth 2008b).

Together, the various contributions to uncertainty in $\nabla \cdot \mathbf{F}_O$ represent a spatially complex pattern of diverse contributions with distinct underlying causes. Despite uncertainty, the principle features of Fig. 7 are larger (order 0.2 PW deg^{-1}) than the combined uncertainty of terms in Fig. 11 (order 0.05 PW deg^{-1}), and thus it is likely that its primary features are robust to data shortcomings. A caveat to these conclusions would be if there is a substantial systematic error across all the estimates for a particular field in Fig. 11. For instance, based on analysis of data from Argo floats, it has recently been suggested that *WOA* overstates the annual cycle in the North Atlantic Ocean (Ivchenko et al. 2006) and perhaps globally (see also Willis et al. 2007).

The potential presence of such biases is particularly likely for ocean analyses, which share both similar analytical bases and observational shortcomings. Revisions of ocean datasets that have been suggested (Ivchenko et al. 2006) would alter the values presented here.

5. Concluding remarks

A test of how well we understand the global energy budget of the earth system and the oceans is to examine the annual cycle in detail and the degree to which closure can be reached among a variety of independent data. Significant advances in the observation and analysis of TOA, atmospheric, and ocean budgets have been made in recent decades such that the errors are now relatively modest and allow for an initial estimate of ocean energy divergence.

In midlatitudes, the seasonal ocean energy tendency is dominated by surface fluxes, with divergence of energy from ocean currents enhancing magnitudes by an order of 50 W m^{-2}. This finding is consistent with model results and is explained by Ekman transports driven by the annual cycle of surface winds. In contrast, in the tropics and subtropics, divergence is found to play the dominant role in the upper-ocean energy budget with secondary but important contributions from surface fluxes.

The first mode of the annual cycle of divergence and the dominant aspects of spatial coherence in this mode are identified and the total transports are calculated, globally and by basin. An additional important implication is that the annual cycle of energy transports is primarily a response to surface winds, rather than instabilities associated with temperature gradients, and it increases seasonal energy extremes in the upper ocean and the amplitude of the annual cycle. This contrasts with the thermohaline circulation, which feeds on density (and thus temperature) gradients.

Inferred annual mean ocean heat transports are somewhat lower than direct ocean estimates in the North Atlantic, and thus the zonal average ocean. Although there are uncertainties in the atmospheric energy transports, there is not much scope for the ocean transports to be increased because their sum is quite strongly constrained. The fields used to infer ocean energy divergence here are indirect and sensitive to the accumulation of error through the depth of the atmosphere and oceans. While retrievals of radiative fluxes of TOA are among the most accurate fields to be observed globally, uncertainty in atmospheric divergence and ocean energy tendency can be substantial, particularly on regional scales. With further refinements of these fields and more complete temporal sampling in the ocean, a more accurate diagnosis of ocean energy divergence will be possible for comparison with model-assimilated fields from analysis of new ocean data. With sufficient data and continued improvements, it will also be possible to extend these kinds of analyses to examine interannual variability. This task has already been realized for the tropical Pacific to examine changes in energy content with ENSO (Trenberth et al. 2002), although improvements in data quality continue to be desirable. With new and improved TOA radiation data from the CERES and much better spatial and temporal resolution from global Argo float measurements, the prospects for doing this diagnosis routinely should become realistic. Accordingly, this approach has the potential to provide a more holistic view of the climate system, help validate ocean models, and better assess the role of ocean energy uptake, release, and transport in climate variability.

Acknowledgments. This research is partially sponsored by the NOAA CLIVAR and CCDD programs under Grants NA06OAR4310145 and NA07OAR4310051. We thank Bill Large, Frank Bryan, and Clara Deser for comments, and Dave Stepaniak for help with computations.

REFERENCES

Antonov, J. I., S. Levitus, and T. P. Boyer, 2004: Climatological annual cycle of ocean heat content. *Geophys. Res. Lett.,* **31,** L04304, doi:10.1029/2003GL018851.

Arnault, S., 1987: Tropical Atlantic geostrophic currents and ship drifts. *J. Geophys. Res.,* **92,** 5076–5088.

Bacon, S., 1997: Circulation and fluxes in the North Atlantic between Greenland and Ireland. *J. Phys. Oceanogr.,* **27,** 1420–1435.

Baringer, M. O., and J. C. Larsen, 2001: Sixteen years of Florida Current transport at 27°N. *Geophys. Res. Lett.,* **28,** 3179–3182.

Barkstrom, B. R., and J. B. Hall, 1982: Earth Radiation Budget Experiment (ERBE)—An overview. *J. Energy,* **6,** 141–146.

Behringer, D. W., 2007: The Global Ocean Data Assimilation System (GODAS) at NCEP. *Proc. 11th Symp. on Integrated Observing and Assimilation Systems for the Atmosphere, Oceans, and Land Surface (IOAS-AOLS),* San Antonio, TX, Amer. Meteor. Soc., 3.3. [Available online at http://ams.confex.com/ams/pdfpapers/119541.pdf.]

——, and Y. Xue, 2004: Evaluation of the global ocean data assimilation system at NCEP: The Pacific Ocean. *Proc. Eighth Symp. on Integrated Observing and Assimilation Systems for Atmosphere, Oceans, and Land Surface,* Seattle, WA, Amer. Meteor. Soc., 2.3. [Available online at http://ams.confex.com/ams/84Annual/techprogram/paper_70720.htm.]

Böning, C. W., and P. Herrmann, 1994: Annual cycle of poleward heat transport in the ocean: Results from high-resolution modeling of the North and equatorial Atlantic. *J. Phys. Oceanogr.,* **24,** 91–107.

Bryden, H. L., D. H. Roemmich, and J. A. Church, 1991: Ocean

heat-transport across 24°N in the Pacific. *Deep-Sea Res.,* **38,** 297–324.

——, H. R. Longworth, and S. A. Cunningham, 2005: Slowing of the Atlantic meridional overturning at 25°N. *Nature,* **438,** 655–657.

Bunker, A. F., 1976: Computations of surface energy flux and annual air–sea interaction cycles of the North Atlantic Ocean. *Mon. Wea. Rev.,* **104,** 1122–1140.

Cunningham, S. A., and Coauthors, 2007: Temporal variability of the Atlantic Meridional Overturning circulation at 26.5°N. *Science,* **317,** 935–938.

Deser, C., M. A. Alexander, and M. S. Timlin, 1999: Evidence for a wind-driven intensification of the Kuroshio Current extension from the 1970s to the 1980s. *J. Climate,* **12,** 1697–1706.

Fasullo, J. T., and K. E. Trenberth, 2008a: The annual cycle of the energy budget. Part I: Global mean and land–ocean exchanges. *J. Climate,* **21,** 2297–2313.

——, and ——, 2008b: The annual cycle of the energy budget. Part II: Meridional Structures and Poleward Transports. *J. Climate,* **21,** 2314–2326.

Ganachaud, A., and C. Wunsch, 2000: Improved estimates of global ocean circulation, heat transport and mixing from hydrographic data. *Nature,* **408,** 453–457.

Grist, J. P., and S. A. Josey, 2003: Inverse analysis adjustment of the SOC air–sea flux climatology using ocean heat transport constraints. *J. Climate,* **16,** 3274–3295.

Hansen, J., and Coauthors, 2005: Earth's energy imbalance: Confirmation and implications. *Science,* **308,** 1431–1435.

Holfort, J., and G. Siedler, 2001: The meridional oceanic transports of heat and nutrients in the South Atlantic. *J. Phys. Oceanogr.,* **31,** 5–29.

Huang, S., 2006: Land warming as part of global warming. *Eos, Trans. Amer. Geophys. Union,* **87,** 477.

Ishii, M., M. Kimoto, K. Sakamoto, and S. I. Iwasaki, 2006: Steric sea level changes estimated from historical ocean subsurface temperature and salinity analyses. *J. Oceanogr.,* **62,** 155–170.

Ivchenko, V. O., N. C. Wells, and D. L. Aleynik, 2006: Anomaly of heat content in the northern Atlantic in the last 7 years: Is the ocean warming or cooling? *Geophys. Res. Lett.,* **33,** L22606, doi:10.1029/2006GL027691.

Jayne, S. R., and J. Marotzke, 2001: The dynamics of ocean heat transport variability. *Rev. Geophys.,* **39,** 385–411.

Kistler, R., and Coauthors, 2001: The NCEP–NCAR 50-Year Reanalysis: Monthly means CD-ROM and documentation. *Bull. Amer. Meteor. Soc.,* **82,** 247–267.

Klein, B., R. L. Molinari, T. J. Muller, and G. Siedler, 1995: A transatlantic section at 14.5n—Meridional volume and heat fluxes. *J. Mar. Res.,* **53,** 929–957.

Kobayashi, T., and N. Imasato, 1998: Seasonal variability of heat transport derived from hydrographic and wind stress data. *J. Geophys. Res.,* **103,** 24 663–24 674.

Köberle, C., and R. Gerdes, 2003: Mechanisms determining the variability of Arctic sea ice conditions and export. *J. Climate,* **16,** 2843–2858.

Koltermann, K. P., A. V. Sokov, V. P. Tereschenkov, S. A. Dobroliubov, K. Lorbacher, and A. Sy, 1999: Decadal changes in the thermohaline circulation of the North Atlantic. *Deep-Sea Res. II,* **46,** 109–138.

Lavin, A., H. L. Bryden, and G. Parrilla, 1998: Meridional transport and heat flux variations in the subtropical North Atlantic. *Global Atmos. Ocean. Syst.,* **6,** 269–293.

Levitus, S., 1984: Annual cycle of temperature and heat storage in the World Ocean. *J. Phys. Oceanogr.,* **14,** 727–746.

——, 1987: Rate of change of heat storage in the World Ocean. *J. Phys. Oceanogr.,* **17,** 518–528.

——, and J. Antonov, 1997: *Climatological and Interannual Variability of Temperature, Heat Storage, and Rate of Heat Storage in the World Ocean*. NOAA Atlas NESDIS 16, 6 pp.+186 figs.

——, ——, and ——, 2005: Warming of the world ocean, 1955–2003. *Geophys. Res. Lett.,* **32,** L02604, doi:10.1029/2004GL021592.

Locarnini, R. A., A. V. Mishonov, J. I. Antonov, T. P. Boyer, and H. E. Garcia, 2006: *Temperature*. Vol. 1, *World Ocean Atlas 2005,* NOAA Atlas NESDIS 61, 182 pp.

Loeb, N. G., and Coauthors, 2007: Multi-instrument comparison of top-of-atmosphere reflected solar radiation. *J. Climate,* **20,** 575–591.

Loschnigg, J., and P. J. Webster, 2000: A coupled ocean–atmosphere system of SST modulation for the Indian Ocean. *J. Climate,* **13,** 3342–3360.

Macdonald, A. M., 1998: The global ocean circulation: A hydrographic estimate and regional analysis. *Prog. Oceanogr.,* **41,** 281–382.

——, and C. Wunsch, 1996: An estimate of global ocean circulation and heat fluxes. *Nature,* **382,** 436–439.

Minster, J. F., A. Cazenave, Y. V. Serafini, F. Mercier, M. C. Gennero, and P. Rogel, 1999: Annual cycle in mean sea level from Topex-Poseidon and ERS-1: Inference on the global hydrological cycle. *Global Planet. Change,* **20,** 57–66.

Moisan, J. R., and P. P. Niiler, 1998: The seasonal heat budget of the North Pacific: Net heat flux and heat storage rates (1950–1990). *J. Phys. Oceanogr.,* **28,** 401–421.

Qiu, B., and R. Lukas, 1996: Seasonal and interannual variability of the North Equatorial Current, the Mindanao Current, and the Kuroshio along the Pacific western boundary. *J. Geophys. Res.,* **101,** 12 315–12 330.

Robbins, P. E., and J. M. Toole, 1997: The dissolved silica budget as a constraint on the meridional overturning circulation of the Indian Ocean. *Deep-Sea Res.,* **44,** 879–906.

Roemmich, D., J. Gilson, B. Cornuelle, and R. Weller, 2001: Mean and time-varying meridional transport of heat at the tropical subtropical boundary of the North Pacific Ocean. *J. Geophys. Res.,* **106,** 8957–8970.

Sato, O. T., and T. Rossby, 2000: Seasonal and low-frequency variability of the meridional heat flux at 36° N in the North Atlantic. *J. Phys. Oceanogr.,* **30,** 606–621.

Saunders, P. M., and B. A. King, 1995: Oceanic fluxes on the WOCE A11 section. *J. Phys. Oceanogr.,* **25,** 1942–1958.

Serreze, M. C., and Coauthors, 2006: The large-scale freshwater cycle of the Arctic. *J. Geophys. Res.,* **111,** C11010, doi:10.1029/2005JC003424.

——, A. P. Barrett, A. G. Slater, M. Steele, J. Zhang, and K. E. Trenberth, 2007: The large-scale energy budget of the Arctic. *J. Geophys. Res.,* **112,** D11122, doi:10.1029/2006JD008230.

Speer, K. G., J. Holfort, T. Reynard, and G. Siedler, 1996: South Atlantic heat transport at 11°S. *The South Atlantic: Present and Past Circulation,* G. Wefer, G. Siedler, and D. J. Webb, Eds., Springer, 105–120.

Talley, L. D., 2003: Shallow, intermediate, and deep overturning components of the global heat budget. *J. Phys. Oceanogr.,* **33,** 530–560.

Trenberth, K. E., 1997: Using atmospheric budgets as a constraint on surface fluxes. *J. Climate,* **10,** 2796–2809.

——, and J. M. Caron, 2001: Estimates of meridional atmosphere and ocean heat transports. *J. Climate,* **14,** 3433–3443.

——, and D. P. Stepaniak, 2003a: Covariability of components of poleward atmospheric energy transports on seasonal and interannual timescales. *J. Climate,* **16,** 3690–3704.

——, and ——, 2003b: Seamless poleward atmospheric energy transports and implications for the Hadley circulation. *J. Climate,* **16,** 3705–3721.

——, and ——, 2004: The flow of energy through the Earth's climate system. *Quart. J. Roy. Meteor. Soc.,* **130,** 2677–2701.

——, J. M. Caron, and D. P. Stepaniak, 2001: The atmospheric energy budget and implications for surface fluxes and ocean heat transports. *Climate Dyn.,* **17,** 259–276.

——, D. P. Stepaniak, and J. M. Caron, 2002: Interannual variations in the atmospheric heat budget. *J. Geophys. Res.,* **107,** 4066, doi:10.1029/2000JD000297.

Uppala, S. M., and Coauthors, 2005: The ERA-40 reanalysis. *Quart. J. Roy. Meteor. Soc.,* **131,** 2961–3012.

Wielicki, B. A., B. R. Barkstrom, E. F. Harrison, R. B. Lee, G. L. Smith, and J. E. Cooper, 1996: Clouds and the Earth's Radiant Energy System (CERES): An earth observing system experiment. *Bull. Amer. Meteor. Soc.,* **77,** 853–868.

——, K. Priestley, P. Minnis, N. Loeb, D. Kratz, T. Charlock, D. Doelling, and D. Young, 2006: CERES radiation budget accuracy overview. Preprints, *12th Conf. on Atmospheric Radiation,* Madison, WI, Amer. Meteor. Soc., 9.1. [Available online at http://ams.confex.com/ams/Madison2006/techprogram/paper_112371.htm.]

Wijffels, S. E., J. M. Toole, H. L. Bryden, R. A. Fine, W. J. Jenkins, and J. L. Bullister, 1996: The water masses and circulation at 10°N in the Pacific. *Deep-Sea Res. I,* **43,** 501–544.

Willis, J. K., D. Roemmich, and B. Cornuelle, 2004: Interannual variability in upper ocean heat content, temperature, and thermosteric expansion on global scales. *J. Geophys. Res.,* **109,** C12036, doi:10.1029/2003JC002260.

——, J. M. Lyman, G. C. Johnson, and J. Gilson, 2007: Correction to "Recent cooling of the upper ocean." *Geophys. Res. Lett.,* **34,** L16601, doi:10.1029/2007GL030323.

Yan, X.-H., P. P. Niiler, S. K. Nadiga, R. Stewart, and D. Cayan, 1995: The seasonal heat storage in the North Pacific. *J. Geophys. Res.,* **100,** 6899–6926.

Zhang, D., W. E. Johns, and T. N. Lee, 2002: The seasonal cycle of meridional heat transport at 24°N in the North Pacific and in the global ocean. *J. Geophys. Res.,* **107,** 3083, doi:10.1029/2001JC001011.